Microchimica Acta (2024) 191:177
https://doi.org/10.1007/s00604-024-06241-3

ORIGINAL PAPER

Point-of-care detection of Monkeypox virus clades using high-performance upconversion nanoparticle-based lateral flow assay

Birui Jin[1,3] · Chuan Ma[1] · Chuyao Zhang[1] · Huiling Yin[3] · Guoxu Zhao[3,4] · Jie Hu[5] · Zedong Li[2,3]

Received: 24 October 2023 / Accepted: 26 January 2024 / Published online: 5 March 2024

Abstract

There is an urgent need for a point-of-care testing (POCT) method in developing and underserved regions to distinguish between two Monkeypox virus (MPXV) clades, given their varying transmissibility and clinical manifestations. In this paper, we target the specific complement protein gene fragment of two MPXV clades and construct a high-performance upconversion nanoparticles–based lateral flow assay (UCNPs-based LFA) with double T-lines and a shared C-line. This enables qualitative and quantitative dual-mode detection when combined with a smartphone and a benchtop fluorescence analyzer. The developed LFA exhibits stable performance, convenient operation, rapid readout (within 8 min), and a much lower limit of detection (LOD) (~ pM level) compared to existing POCT methods. The proposed detection platform demonstrates significant potential for pathogen diagnosis using a POCT approach.

Keywords Point-of-care testing · Lateral flow assay · Fluorescence · Monkeypox virus · Nucleic acid detection

Introduction

The Monkeypox virus (MPXV) outbreaks have spread to 117 nations [1], creating a significant burden on human health and society. MPXV strains are broadly categorized into two genetic clades: the Congo Basin clade, associated with higher virulence but reduced transmissibility, and the West African clade, characterized by lower virulence yet higher prevalence [2–4]. Hence, distinguishing between these two clades at point-of-care is of significance for implementing clinical interventions.

Nucleic acid detection, a commonly used method for virus detection, can effectively differentiate MPXV from other orthopoxviruses by targeting specific gene fragments with distinct signature [5]. Notably, the specific complement binding protein genes, C3L (pertinent to the former Congo Basin clade) and G2R_WA (specific to the West African clade), have proven valuable for discerning these two clades [6]. Laboratory-based polymerase chain reaction (PCR) technique has shown high sensitivity and accuracy in detecting such two clades [7, 8]. Nonetheless, the necessity for multiple rounds of thermal cycling renders such method intricate, cost-intensive, and time-consuming. As a remedy, many isothermal amplification methods (e.g., recombinase polymerase amplification [9]) have been developed for MPXV detection. By eliminating the thermal cycling requirement, these methods significantly diminish the detection expenses and operational complexity [10]. However, due to the affection of reaction time and inhibition effect to amplification degree, these strategies suffer from the limitations in accuracy and quantification [11].

✉ Jie Hu
jason.hu@sz-dna.cn

✉ Zedong Li
zedong@xjtu.edu.cn

1 School of Materials and Chemical Engineering, Xi'an Technological University, Xi'an 710021, People's Republic of China

2 Key Laboratory of Shaanxi Province for Craniofacial Precision Medicine Research, College of Stomatology, Xi'an Jiaotong University, Xi'an, People's Republic of China

3 Bioinspired Engineering and Biomechanics Center (BEBC), Xi'an Jiaotong University, Xi'an 710049, People's Republic of China

4 State Key Laboratory of Digital Medical Engineering, School of Biomedical Engineering, Hainan University, Haikou 570228, People's Republic of China

5 Suzhou DiYinAn Biotech Co., Ltd., Suzhou Innovation Center for Life Science and Technology, Suzhou 215129, People's Republic of China

Lateral flow assay (LFA) has been widely developed as a rapid, cost-effective, and user-friendly detection platform for recognizing viruses, including COVID-19, influenza, Ebola, Zika, and dengue viruses [12–15]. However, the conventional color reporters used in LFAs, such as AuNPs [16] and AgNPs [17], often yield weak signals, leading to insufficient sensitivity in nucleic acid testing for distinguishing viruses. The advancement in novel labeling nanomaterials, particularly fluorescent nanoparticles like fluorescent dyes [18], fluorescent microspheres [19], quantum dots [20], and upconversion nanoparticles (UCNPs) [14], has marked a breakthrough in this field [21]. These materials offer stronger and more quantifiable detection signals, greatly improving the detection sensitivity and accuracy of LFAs. Notably, the utilization of UCNPs with their unique anti-Stokes properties offers a solution to effectively avoid background fluorescence, enabling them an excellent nanomaterial for labeling and detecting [22]. Numerous LFAs developed using UCNPs exhibit prolonged fluorescence stability and an elevated signal-to-noise ratio [23], which have been effectively employed for detection of various targets with robust detection capability, such as bacteria [23], biotoxin [24], and metal ions [25]. Furthermore, when coupled with optimization strategies, such as regulation of fluorescence intensity and surface probe density [26], the detection performance of UCNPs-based LFA can be further improved to expand their utilization.

This study uses UCNPs with high fluorescent intensity to create a high-performance LFA with double T-lines and a shared C-line, which is capable of simultaneously detecting two clades of MPXV. The resulting platform enables both convenient at-home virus screening using a smartphone and highly sensitive laboratory detection utilizing a benchtop fluorescence analyzer. This dual-mode detection offers the benefits of cost-effectiveness, user-friendliness, and broad applicability.

Materials and methods

Materials

$Y(CF_3COO)_3$, $Yb(CF_3COO)_3$, and $Er(CF_3COO)_3$ were prepared by Suzhou University. Sodium trifluoroacetate, 1-Octadecene (ODE), oleic acid (OA), and N-Hydroxysulfosuccinimide sodium salt (Sulfo-NHS) were purchased from Aladdin. N-(3-dimethylaminopropyl)-N′-ethylcarbodiimide hydrochloride crystalline (EDC), Trizma base (Tris), and Proclin 300 were obtained from Sigma Aldrich. Ethanol absolute, cyclohexane, chloroform, dimethyl sulfoxide (DMSO), and glycine were obtained from Sinopharm Group Chemical Reagent Co., Ltd. HEPES, MES, and BSA were obtained from Solarbio. DSPE-PEG-COOH and Streptavidin were obtained from Xi'an Ruixi Biotechnology Company and Shanghai Maclin Biochemical Technology Co., Ltd, respectively. Nucleic acid sequences of MPXV and their probe sequences were synthesized by Sangong Bioengineering (Shanghai) Co., Ltd (Table 1). All reagents are analytical grade. The components of LFA, including sample pad (SB08), absorbent pad (H-1), immersing pad (8965), nitrocellulose (NC) membrane (Sartorius CN 95), and PVC backing pad, were bought from Shanghai Jening Biotechnology Co., Ltd.

Preparation and modification of $NaYF_4$: Yb^{3+}, Er^{3+}

The UCNPs ($NaYF_4$: Yb^{3+}, Er^{3+}) were synthesized using thermal decomposition method, according to our last paper [26]. Details were shown in the Supplementary materials.

Nucleic acid probe modification on UCNP surface

The two kinds of recognition probes were designed according to the specific nucleic acid fragments of two clades of MPXV (C3L and G2R_WA) reported in the literature, and the sequences were shown in Table 1. The amino modified

Table 1 The sequences of two MPXV clades and their corresponding detection probe

Name	Sequence (5'–3′)
G2R_WA target	CACACCGTCTCTTCCACAGATAAATGCGAACTATATCGATGTGGAAATTAACCTGTATC
G2R_WA recognition probe	TCTGTGGAAGAGACGGTGTG/PEG_9/A_{10}/NH_2
G2R_WA capture probe	Biotin/GATACAGGTTAATTTCCACATCG
G2R_WA control probe	CACACCGTCTCTTCCACAGA/Biotin
C3L target	TGTCTACCTGGATACAGAAAGCAAAAAATGGGATGGACACTCTTTAATCAATGTATT AAACGGAGATGCC
C3L recognition probe	TTGCTTTCTGTATCCAGGTAGACA/PEG_9/A_{10}/NH_2
C3L capture probe	Biotin/GGCATCTCCGTTTAATACATTGAT
C3L control probe	TGTCTACCTGGATACAGAAAGCAA/Biotin

G2R_WA and C3L recognition probes were conjugated to water-soluble UCNPs by a condensation reaction to form UCNPs-probes. Specifically, the as-prepared PEG@UCNPs (40 μL) were mixed with MES buffer (20 mM, pH = 6.0) in a ratio of 1:2 (v/v). EDC and Sulfo-NHS (5 μL, 24 mg/mL) were added for carboxyl group activation. The mixture was placed in a constant temperature shaker (37 °C, 45 min, 220 rpm). After resuspension in 0.6 mL MES buffer, recognition probes (120 μL, 100 nM) modified with amino group were added to continue the reaction in the shaker for 2 h. Furthermore, 18 μL sealing buffer (15% Glycine, 1% Proclin 300, pH = 11) was added to complete site sealing. The products (UCNPs-probes) were washed and resuspended in 0.6 mL probe-diluent (0.5% v/v Tween 20, 4% (w/v) BSA and SSC (2×), pH = 7.0).

Construction of UCNPs-based LFA

The UCNPs-based LFA was prepared according to the literature [27]. For single-target detection, UCNPs-probes for C3L clade or G2R_WA clade were evenly sprayed (5 μL/cm) on the immersing pad. To form T-lines and C-line, biotin-modified capture probes and control probes were fixed on NC membrane using streptavidin as intermediate. The corresponding capture probes and control probes were sprayed on the NC membrane with a dosage of 1 μL/cm. Each component was dried for 2 h at 37 °C. Then, the NC membrane, sample pad, immersing pad, and absorbent pad were pasted onto a PVC backing pad with an overlap of 2 mm. The pasted pads were cut into strips with a 3.9 mm width by programmable shear. For dual-target detection, the approach is to spray G2R_WA and C3L UCNPs-probes mixed on immersing pad, build two T-lines with two clades of capture probes, and mix the control probes of two clades at 0.5 times the original concentration to build a mixed C-line.

Detection of single MPXV

To evaluate the detection capabilities of the UCNPs-based LFA, we prepared standard samples of MPXV (G2R-WA and C3L) with gradient concentrations (0, 0.001, 0.01, 0.1, 0.5, 5, 25, 50, 100 nM). The procedure involved mixing 50 μL sample with 50 μL optimized sample-diluent, which was then applied to the designated sample area. After an 8-min reaction, the fluorescence signals on both T-line and C-line were read and analyzed. For reading results via a smartphone camera under darkroom conditions, specific parameters including a shutter speed of 1/200 and ISO 2600 were applied. Similarly, the benchtop fluorescence analyzer we developed could quantitatively assess the fluorescence intensity of each dot within the detection area and translate them into a peak graph. Each target concentration was repeated 3 times, while the blank sample underwent ten repetitions. Employing the mean value and standard deviation, a standard curve was fitted, and the detection limit was calculated according to the formula (S/N = 3).

Simultaneous detection of two clades of MPXV

A dual-target LFA was developed by integrating two single-target UCNPs-based LFAs. This involved mixing the G2R_WA and C3L UCNPs-probes and applying them to the binding pad. Two separate T-lines were created using their respective capture probes, and a new C-line was formed by mixing the two control probes at half concentration. The performance of this dual-target LFA was evaluated using standard samples of G2R_WA and C3L targets. The detection process remained consistent with the previously described method.

Detection of spiked sample

Spiked serum samples of G2R-WA and C3L targets at different concentrations (0, 0.1, 0.5, 2.5, 5, 10, 25 nM) were introduced to test the anti-interference capability of the developed UCNPs-based LFA. The 50 μL as-prepared spiked serum samples were mixed with sample-diluent in a ratio of 1:1 and then detected 3 times using the developed LFA.

Furthermore, plasmids representing MXPV were designed by Basic Local Alignment Search Tool (BLAST). The forward and reverse primers and plasmids were synthesized by Sangong Bioengineering (Shanghai) Co., Ltd. The plasmids with different concentrations (10^3, 10^4, 10^5 copies/μL) were amplified using qPCR (Jena, qTOWER3). The reaction conditions were as follows: pre-denaturation at 95 °C for 5 min, followed by 45 cycles of 20 s denaturation at 95 °C and 30 s annealing at 60 °C. An asymmetric amplification model was implemented with a 10×Primer Mix and an 8:1 ratio of forward primers to reverse primers to generate more free single strands. The resulting amplified products, mixed with 80 μL sample dilution, were detected using the developed LFA 3 times.

Results and discussion

Development of high-performance POCT platform for MPXV

The detection principle of MPXV using a UCNPs-based LFA was shown in Fig. 1. Utilizing UCNPs with a larger particle size can effectively enhance the fluorescence signal intensity in detection due to their increased fluorescence intensity and greater surface modification capability. As a result, UCNPs with a diameter size of 500 nm were adopted to construct high-performance LFA. The developed

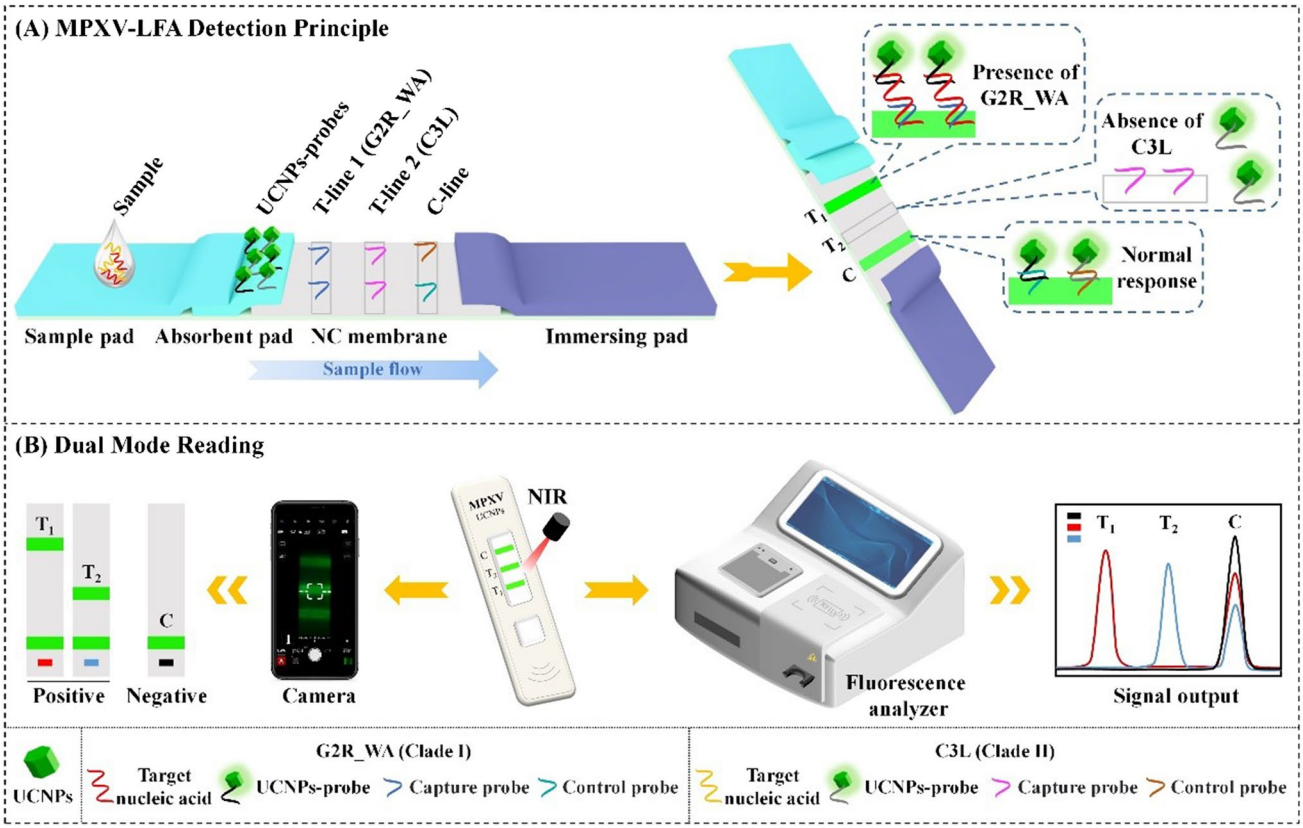

Fig. 1 The principle of the UCNPs-based LFA for dual MPXV detection. **A** The structure and detection principle of UCNPs-based LFA. **B** The dual-mode reading using a smartphone and a fluorescence analyzer

UCNPs-based LFA operates on a sandwich strategy. As depicted in Fig. 1A, the presence of the target triggers the corresponding T-line to emit fluorescence signals, which can be read and analyzed through a dual-mode approach. The fluorescence images, achieved using a smartphone camera in conjunction with a 980-nm laser, exhibit clear bands that can be easily discerned with the naked eyes, enabling straightforward and portable at-home self-testing. In addition, the fluorescence signal on the LFA can be scanned point-by-point using a custom benchtop fluorescence analyzer to form a fluorescence peak graph, facilitating precise and sensitive quantitative analysis. Each peak fluorescence intensities correspond to detection signals of each T-line or C-line (Fig. 1B).

Characterization of UCNPs

The sensitivity and stability of UCNPs-based LFA are closely related to the fluorescence intensity, size uniformity, and conjugation capability of UCNPs. $NaYF_4$ was selected as the matrix material due to the low phonon energy and high chemical stability, and Yb^{3+} and Er^{3+} were chosen as activators and sensitizers with molar concentration ratios of 18% and 2%. To obtain large-size UCNPs, the heating time at 320 °C was extended to 110 min during the synthesis process. This adjustment reduced the surface quenching and greatly improved the fluorescence intensity. In particular, UCNPs with a large size (500 nm) exhibited superior detection performance owing to their larger surface area and stronger fluorescence intensity, as indicated in our prior publication [26]. To validate the characteristics of the synthesized UCNPs, we conducted analyses on their composition, morphology, size, and fluorescence intensity. XRD patterns (Fig. 2A) confirm that the diffraction peaks of the synthesized UCNPs match those of the standard card (β-$NaYF_4$, JCPDS no. 16–0334). Morphological insights from TEM (Fig. 2B) illustrate that the prepared UCNPs exhibit uniform hexagonal prism shapes with an average size of 500 nm. The UCNPs emit a vibrant green fluorescence under 980 nm excitation light (inset of Fig. 2C). The fluorescence spectra consistent with the standard emission spectra of $NaYF_4$: Yb, Er, which reveal emission peaks at 540 nm and 650 nm (Fig. 2C). Due to the stronger intensity, the 540 nm emission peak serves as the primary analysis signal in this developed platform. In addition, a recognition probe concentration of 0.36 nM was chosen for UCNP conjugation.

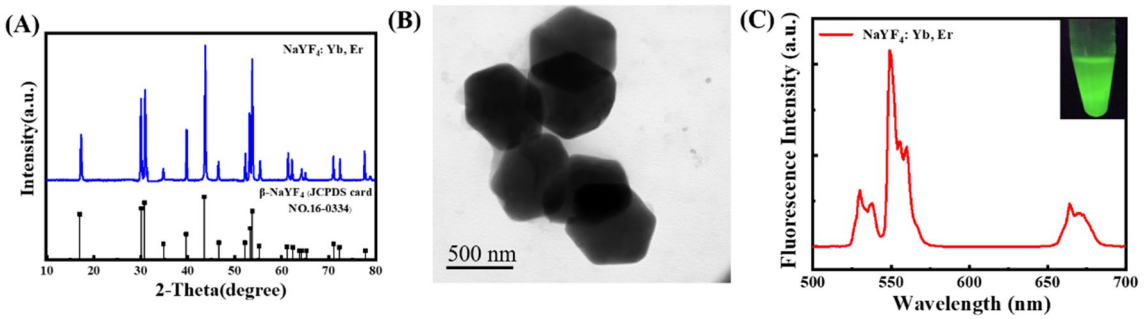

Fig. 2 Characterization of UCNPs. **A** XRD patterns, **B** TEM photo, and **C** fluorescence spectra of UCNPs

Detection validation of the UCNPs-based LFA

The real product of constructed LFA is shown in Fig. 3A. After being dropped on sample area, a 100 µL of sample flows through the detection area together with UCNPs-probes on the immersing pad. This process leaves behind discernible signals on T-line and C-line after undergoing corresponding reactions. Under the 980-nm excitation light, the detection area displays prominent green fluorescent bands that are markedly distinguished from the background, proving a high signal-to-noise ratio. Evidently, with an increase in the target concentration, the T-line signal rises while the C-line signal decreases. This occurs because more UCNPs are captured at the T-line, and fewer flow through the C-line. In addition, the fluorescence signal of the detection can be read by a custom benchtop fluorescence analyzer

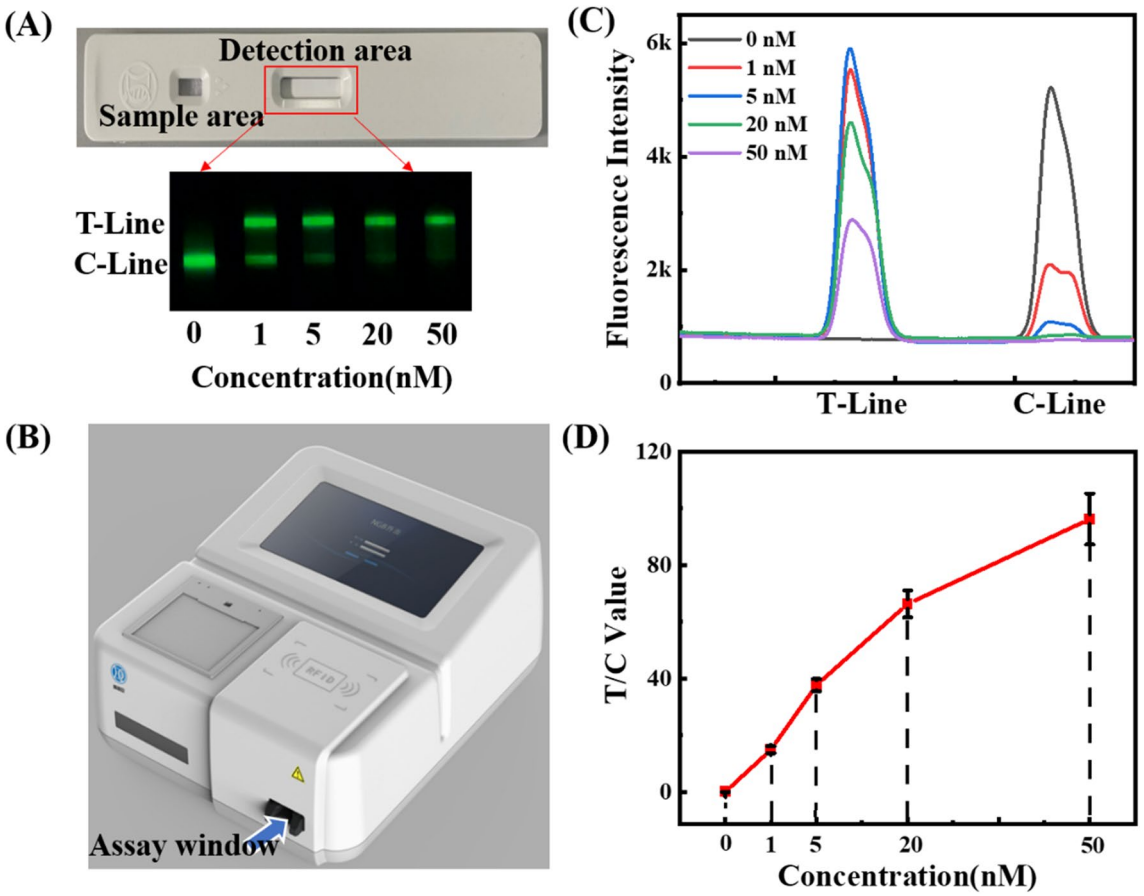

Fig. 3 UCNPs-based LFA platform for MPXV detection. **A** Real product of LFA and its fluorescence photos. **B** Real product of benchtop fluorescence analyzer. **C** Scanned by benchtop fluorescence analyzer, the relationship graph of fluorescence intensity, and scanning position with different target concentrations. **D** The relationship graph of quantized T/C value and target concentration

(Fig. 3B). The detail structure of the benchtop fluorescence analyzer was shown in our previous work [26]. The relationship curve of fluorescence intensity and scanning position was constructed to yield quantitative analytical outcomes (Fig. 3C), with an analysis procedure outlined in the Supplementary materials. Finally, the quantized T/C value (integral area ratio of T-line and C-line peak) serves as the detection signal to shape the concentration-signal graph (Fig. 3D), which shows a good linear upward trend and differentiation degree in the detection area. It is noteworthy that since the C-line signal also varies with the target concentration, utilizing the T/C value as the analysis result can effectively enhance the stability and signal differentiation of the system.

Development of a high-performance LFA platform

To enable the developed LFA platform to achieve better detection performance, variety parameters were optimized. Firstly, a precisely tailored sample dilution effectively mitigates false positives, prevents non-specific binding on NC membrane, and significantly improves the signal-to-noise ratio for both MPXV clades. The optimized sample dilution recipe consists of HEPES (2.383%, w/v, pH = 8), NaCl (1.58%, w/v), BSA (5%, w/v), Tween 20 (5%, v/v), EDTA (0.0465%, w/v), and Glycine (15%, w/v). Furthermore, the concentration of probes modified on the T-line and C-line also profoundly impacts the strength of the fluorescence signal, thereby influencing the accuracy of result interpretation. Our experimental findings determined the optimal T-line and C-line dosages is 100 μM and 75 μM, respectively. A reduced probe concentration on C-line can result in a more pronounced change in the C-line signal with respect to the target. The concentration of UCNPs-probes exerts an impact on their binding capability to the target, which consequently influences the signal-to-noise ratio and the sensitivity of LFA. To further optimize the performance of the developed platform, the concentration of UCNPs-probes was regulated (Fig. S1). It is evident that G2R_WA and C3L both exhibit an optimum detection range and LOD at 2 × UCNPs-probes concentration (1 × concentration: 3.3 mg/mL).

Separate detection of two clades of MPXV

To verify the detection performance of UCNPs-based LFA, detections were performed using G2R_WA and C3L standard samples with gradient concentrations. Each target concentration was tested 3 times, while the blank sample underwent ten repetitions. As the fluorescence signals stabilized after an 8-min reaction, the detection signals at 8 min were chosen for analysis (Fig. S2). Taking G2R_WA detection as an example, as depicted in the fluorescence photos (Fig. 4A), within the target concentration range of 0.01–50 nM, the T-line fluorescence signals initially increased and then attenuated with rising target concentration. In contrast, the C-line fluorescence signal gradually weakened, and notable background fluorescence was absent. This smartphone-based reading approach is straightforward to execute and equipment-free, enabling qualitative detection within a certain range.

Moreover, the benchtop fluorescence analyzer permits quantification of the fluorescence signals emanating from both T-line and C-line, forming distinctive peak patterns (Fig. 4B). Through mathematical fitting, these quantified fluorescence signal values (T/C value) can be correlated with the target concentration to achieve accurate quantitative detection. Especially, the fluorescence signal, which may not be discernible in fluorescence photos, become readily measurable on the peak pattern, substantiating the fluorescence reader's capability to capture lower-level detection signals. The standard curve for both clades (Fig. 4C–D) exhibits a strong linear correlation ($R^2 = 0.999$). Repeated experiments revealed an average coefficient of variation (CV) of less than 15% for both clades, meeting the stability criteria. The LOD for both qualitative or quantitative analysis was calculated using the formula S/N = 3 (defined as blank + 3 std dev of the blank), yielding an LOD of 0.6 pM for G2R_WA and an LOD of 1 pM for C3L, respectively. For qualitative analysis, signal is taken from the average grey-value in green channel of the T-line region in the fluorescence photograph. For quantitative analysis, the quantified fluorescence intensity can be read directly by the fluorescence analyzer. In detail, the obtained signal is greater than 3 times the standard deviation of blank can be recognized as coming from the target rather than the systematic error. This represents a substantial enhancement in sensitivity compared to relevant POCT nucleic acid detection methods operating at the nanomolar (nM) level [28–30]. To assess the stability of the developed UCNPs-based LFA, LFAs from the same batch were stored at room temperature (25 °C). Furthermore, the stability of the developed UCNPs-based LFA has been demonstrated over a 20-day period under room temperature storage conditions (Fig. S3).

Integration for both two clades of MPXV detection

The above results serve to validate the constructed UCNPs-based LFA platform's notable sensitivity and stability in independently detecting the two MPXV clades. To further substantiate the dual-target detection capability of developed LFA, the detection of both G2R_WA and C3L was integrated into a single LFA setup. The results from the dual-target detection are shown in Fig. 5A. No peaks are observable in T-line 1 and T-line 2 in the control group, indicating the absence of false positives in the dual-target detection. Upon the addition of a target, the corresponding T-line manifests a peak value that varies with concentration, while the other

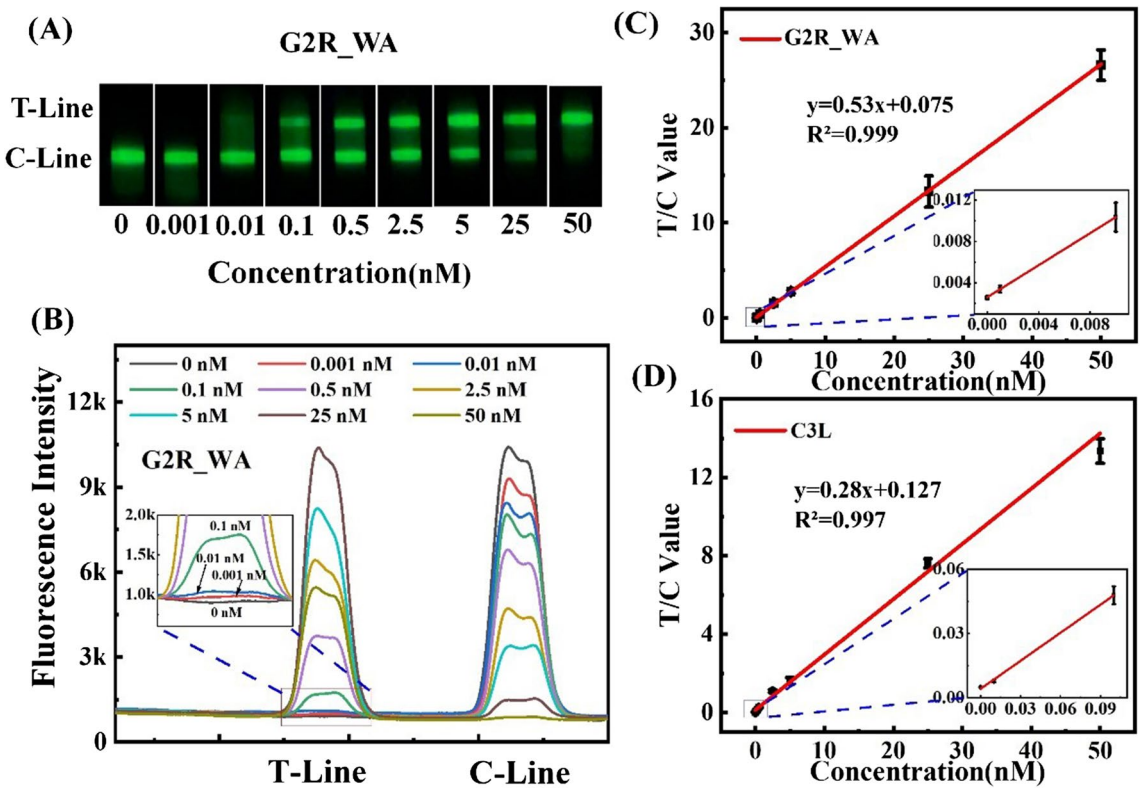

Fig. 4 Detection of two clades of MPXV separately. **A** Fluorescence photos and **B** peak patterns of G2R_WA with gradient concentration. The standard curve of **C** G2R_WA clade and **D** C3L clade. The fitted standard curves are $y=0.53x+0.075$ (G2R_WA) and $y=0.28x+0.127$ (C3L), respectively

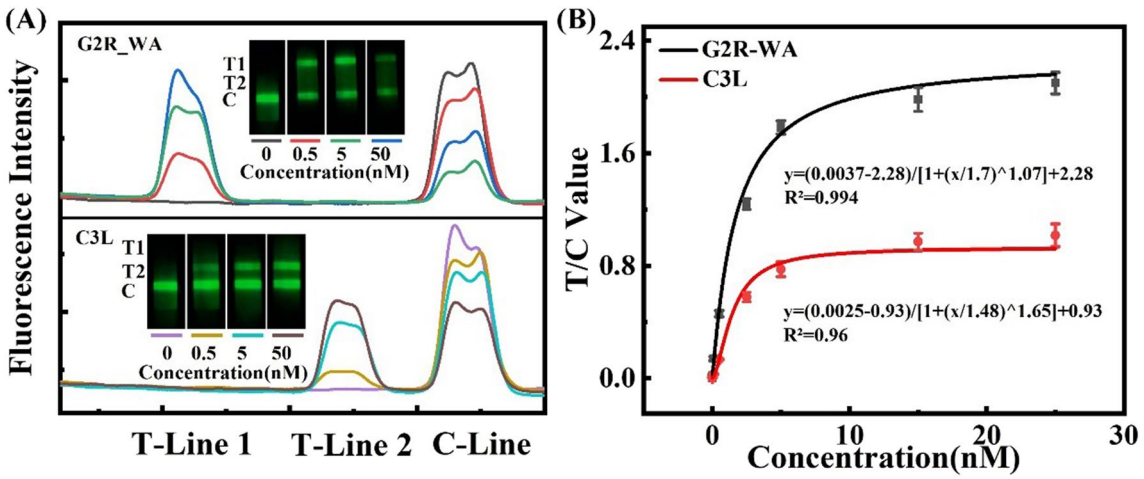

Fig. 5 Integration for both two clades of MPXV detection. **A** Fluorescence photos and peak patterns of dual-target detection. **B** Standard curves of dual-target detection

T-line remains devoid of any signal, affirming the absence of cross-reaction within the dual-target detection system.

Differing from single-target detection, the C-line signal in the dual-target scenario is influenced by both clade-specific fluorescence probes. Even at higher target concentrations, the C-line retains elevated signals, resulting in a small T/C value. Therefore, new standard curves were established for the dual-target detection through four-parameter fitting (Fig. 5B). According to the new standard curves, the LOD for dual-target detection is 0.9 pM

(G2R_WA) and 1.2 pM (C3L), with upper limits reaching 25 nM for both G2R_WA and C3L. Remarkably, these values are not significantly different from those achieved in single-target detection. These findings collectively demonstrate that the dual-target LFA can accurately and effectively discern the presence of MPXV infection and identify the specific clades, offering a heightened detection performance when compared to existing POCT methods. Through comparison with other LFA-based methods for MPXV nucleic acid detection (Table S1), although our method has the advantage of a rapid readout, the LOD is not comparable to other LFAs with nucleic acid amplification pretreatment. To our knowledge, this is the first POCT method for simultaneous detection of G2R and C3L on a single LFA. Additionally, compared to other optical LFAs developed for nucleic acid detection without amplification (Table S2), our method has considerable competitiveness in terms of LOD and detection time.

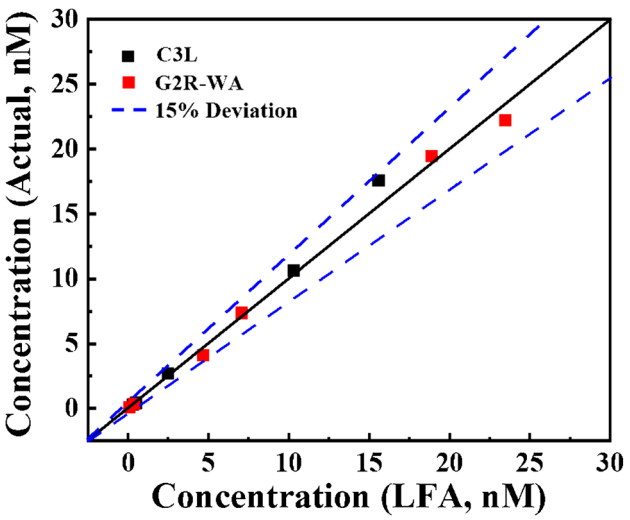

Fig. 6 Practical application validation of UCNPs-based LFA detection in spiked serum sample. The area between the two dashed lines indicates the range where the deviation is less than 15%

Practical application validation

To evaluate the anti-interference ability of the developed UCNPs-based LFA in real application, we introduced a series of gradient concentrations of G2R-WA and C3L into human serum as spiked clinical samples. By establishing the correlation between fluorescence intensity and target concentration, the detection results were compared with the actual results (Fig. 6). The findings demonstrated that all detection outcomes fell within the range defined by the two dashed lines (± 15%), which is indicated to meet the common requirement of POCT. This suggests that the established UCNPs-based LFA platform is suitable for application in serum samples detection.

To further validate the practical detection capabilities of the developed LFA, we designed plasmids to replace MPXV as clinical samples using the Basic Local Alignment Search Tool (BLAST). Plasmid samples with different concentrations (10^3, 10^4, 10^5 copies/μL) were amplified using qPCR for 45 cycles. An asymmetric amplification model was performed with 10 × primer Mix and an 8:1 ratio of forward primers to reverse primers to produce more free single strands. The obtained results (Table 2) show that the detection outcomes of the UCNPs-based LFA can still align with the individual actual concentrations, with a deviation of less than ± 15%. This capability enables the detection of low concentrations, down to 10^3 copies/μL. Collectively, these findings substantiate the effective applicability of the developed UCNPs-based LFA platform for practical applications.

In summary, the developed platform demonstrates greater suitability for point-of-care testing scenarios by effectively eliminating biological sample interference, reducing detection time, and enhancing detection sensitivity through cost-effective methods. However, it remains crucial to integrate amplification technology to fully meet the demands of detecting low-abundance clinical samples. This highlights a prospective research direction for us: incorporating targeted enrichment methods or cyclic reaction systems to genuinely achieve clinical applications without amplification.

Table 2 Clinical validation of UCNPs-based LFA for detection in MPXV plasmid samples

MPXV branch	Actual concentration (copies/μL)	Cycle number (times)	Detection concentration (copies/μL)	Coefficient variation (%)
G2R-WA	0	45	-	-
	10^3		9.88×10^2	− 1.12%
	10^4		1.05×10^4	5.70%
	10^5		8.71×10^4	− 12.87%
C3L	0		-	-
	10^3		1.03×10^3	3.86%
	10^4		8.97×10^3	− 10.20%
	10^5		9.38×10^4	− 6.11%

Conclusion

Utilizing UCNPs with enhanced fluorescence intensity and greater probe modification capacity, this study has developed a high-performance LFA with double T-lines and a shared C-line, offering both qualitative and quantitative dual-mode detection options through smartphone-based reading and a benchtop fluorescence analyzer. The resulting UCNPs-based LFA demonstrates remarkable sensitivity, rapidity, and stability, which can achieve an LOD of 0.9 pM (G2R_WA) and 1.2 pM (C3L) of two MPXV clades within 8 min. In addition, the spiked sample detection proved that the developed detection platform has excellent anti-interference and can realize the MPXV detection. This validates the proposed UCNPs-based LFA's potential for rapid identification of the presence and specific clade of MPXV infection. Although the strategy showcases considerable potential in the field of nucleic acid detection, it is still necessary to combine amplification techniques to meet the detection needs of real clinical samples. This points out the future research direction in this area. Enrichment or cyclic reactions may be used to further optimize sensitivity, and really achieve non-amplification detection, and eliminate the impact of primer design, amplification procedures, and equipment.

Supplementary Information The online version contains supplementary material available at https://doi.org/10.1007/s00604-024-06241-3.

Funding This work was supported by the Opening Research Fund from Key Laboratory of Shaanxi Province for Craniofacial Precision Medicine Research, College of Stomatology, Xi'an Jiaotong University (2019LHM-KFKT005); the General Financial Grant from the China Postdoctoral Science Foundation (2020M673418); the Natural Science Foundation of the Anhui Higher Education Institutions of China (KJ2021ZD0150); and the National Natural Science Foundation of China (61904143).

Declarations

Conflict of interest The authors declare no competing interests.

References

1. WHO (2023) 2022–23 Mpox (Monkeypox) outbreak: global trends. https://worldhealthorg.shinyapps.io/mpx_global/. Accessed 25 Jan 2024
2. WHO (2022) Monkeypox: experts give virus variants new names. https://www.who.int/news/item/12-08-2022-monkeypox--experts-give-virusvariants-new-names. Accessed 13 Aug 2022
3. Lai C-C, Hsu C-K, Yen M-Y, Lee P-I, Ko W-C, Hsueh P-R (2022) Monkeypox: an emerging global threat during the COVID-19 pandemic. J Microbiol Immunol Infect 55:787–794. https://doi.org/10.1016/j.jmii.2022.07.004
4. McCollum AM, Damon IK (2014) Human monkeypox. Clin Infect Dis 58:260–267. https://doi.org/10.1093/cid/ciu196
5. Zandi M, Adli AH, Shafaati M (2022) Comments on "diagnosis of monkeypox virus—an overview." Travel Med Infect Dis 51:102511. https://doi.org/10.1016/j.tmaid.2022.102511
6. Li Y, Zhao H, Wilkins K, Hughes C, Damon IK (2010) Real-time PCR assays for the specific detection of monkeypox virus West African and Congo Basin strain DNA. J Virol Methods 169:223–227. https://doi.org/10.1016/j.jviromet.2010.07.012
7. Li Y, Olson VA, Laue T, Laker MT, Damon IK (2006) Detection of monkeypox virus with real-time PCR assays. J Clin Virol 36:194–203. https://doi.org/10.1016/j.jcv.2006.03.012
8. Sharkey ME, Babler KM, Shukla BS, Abelson SM, Alsuliman B, Amirali A, Comerford S, Grills GS, Kumar N, Laine J (2023) Monkeypox viral nucleic acids detected using both DNA and RNA extraction workflows. Sci Total Environ 890:164289. https://doi.org/10.1016/j.scitotenv.2023.164289
9. Cui X, Du B, Feng J, Feng Y, Cui J, Yan C, Zhao H, Gan L, Fan Z, Fu T (2023) Rapid detection of mpox virus using recombinase aided amplification assay. Front Cell Infect Microbiol 13:145. https://doi.org/10.3389/fcimb.2023.1008783
10. Gul I, Liu C, Yuan X, Du Z, Zhai S, Lei Z, Chen Q, Raheem MA, He Q, Hu Q (2022) Current and perspective sensing methods for monkeypox virus. Bioengineering 9:571. https://doi.org/10.3390/bioengineering9100571
11. Rohrman B, Richards-Kortum R (2015) Inhibition of recombinase polymerase amplification by background DNA: a lateral flow-based method for enriching target DNA. Anal Chem 87:1963–1967. https://doi.org/10.1021/ac504365v
12. You M, Lin M, Gong Y, Wang S, Li A, Ji L, Zhao H, Ling K, Wen T, Huang Y (2017) Household fluorescent lateral flow strip platform for sensitive and quantitative prognosis of heart failure using dual-color upconversion nanoparticles. ACS Nano 11:6261–6270. https://doi.org/10.1021/acsnano.7b02466
13. Corstjens PL, De Dood CJ, Kornelis D, Fat EMTK, Wilson RA, Kariuki TM, Nyakundi RK, Loverde PT, Abrams WR, Tanke HJ (2014) Tools for diagnosis, monitoring and screening of Schistosoma infections utilizing lateral-flow based assays and upconverting phosphor labels. Parasitology 141:1841–1855. https://doi.org/10.1017/S0031182014000626
14. Martiskainen I, Talha SM, Vuorenpää K, Salminen T, Juntunen E, Chattopadhyay S, Kumar D, Vuorinen T, Pettersson K, Khanna N (2021) Upconverting nanoparticle reporter–based highly sensitive rapid lateral flow immunoassay for hepatitis B virus surface antigen. Anal Bioanal Chem 413:967–978. https://doi.org/10.1007/s00216-020-03055-z
15. Guo J, Chen S, Tian S, Liu K, Ma X, Guo J (2021) A sensitive and quantitative prognosis of C-reactive protein at picogram level using mesoporous silica encapsulated core-shell up-conversion nanoparticle based lateral flow strip assay. Talanta 230:122335. https://doi.org/10.1016/j.talanta.2021.122335
16. Xu S, Zhang G, Fang B, Xiong Q, Duan H, Lai W (2019) Lateral flow immunoassay based on polydopamine-coated gold nanoparticles for the sensitive detection of zearalenone in maize. ACS Appl Mater Interfaces 11:31283–31290. https://doi.org/10.1021/acsami.9b08789
17. Wu K-H, Huang W-C, Chang S-C, Shyu R-H (2022) Colloidal silver-based lateral flow immunoassay for detection of profenofos pesticide residue in vegetables. RSC Adv 12:13035–13044. https://doi.org/10.1039/D2RA01654K
18. Lou D, Fan L, Jiang T, Zhang Y (2022) Advances in nanoparticle-based lateral flow immunoassay for point-of-care testing. View 3:20200125. https://doi.org/10.1002/VIW.20200125
19. Jiang J, Luo P, Liang J, Shen X, Lei H, Li X (2022) A highly sensitive and quantitative time resolved fluorescent microspheres lateral flow immunoassay for streptomycin and dihydrostreptomycin in milk, honey, muscle, liver, and kidney. Anal Chim Acta 1192:339360. https://doi.org/10.1016/j.aca.2021.339360

20. Wang C, Yang X, Gu B, Liu H, Zhou Z, Shi L, Cheng X, Wang S (2020) Sensitive and simultaneous detection of SARS-CoV-2-specific IgM/IgG using lateral flow immunoassay based on dual-mode quantum dot nanobeads. Anal Chem 92:15542–15549. https://doi.org/10.1021/acs.analchem.0c03484
21. Zhang J, Shikha S, Mei Q, Liu J, Zhang Y (2019) Fluorescent microbeads for point-of-care testing: a review. Microchim Acta 186:1–21. https://doi.org/10.1007/s00604-019-3449-y
22. Brandmeier JC, Raiko K, Farka Z, Peltomaa R, Mickert MJ, Hlaváček A, Skládal P, Soukka T, Gorris HH (2021) Effect of particle size and surface chemistry of photon-upconversion nanoparticles on analog and digital immunoassays for cardiac troponin. Adv Healthcare Mater 10:2100506. https://doi.org/10.1002/adhm.202100506
23. Gong Y, Zheng Y, Jin B, You M, Wang J, Li X, Lin M, Xu F, Li F (2019) A portable and universal upconversion nanoparticle-based lateral flow assay platform for point-of-care testing. Talanta 201:126–133. https://doi.org/10.1016/j.talanta.2019.03.105
24. Jin B, Li Z, Zhao G, Ji J, Chen J, Yang Y, Xu R (2022) Upconversion fluorescence-based paper disc for multiplex point-of-care testing in water quality monitoring. Anal Chim Acta 1192:339388. https://doi.org/10.1016/j.aca.2021.339388
25. Sivakumar R, Lee NY (2021) Recent progress in smartphone-based techniques for food safety and the detection of heavy metal ions in environmental water. Chemosphere 275:130096. https://doi.org/10.1016/j.chemosphere.2021.130096
26. Jin B, Du Z, Ji J, Bai Y, Tang D, Qiao L, Lou J, Hu J, Li Z (2023) Regulation of probe density on upconversion nanoparticles enabling high-performance lateral flow assays. Talanta 256:124327. https://doi.org/10.1016/j.talanta.2023.124327
27. Jin B, Yang Y, He R, Park YI, Lee A, Bai D, Li F, Lu TJ, Xu F, Lin M (2018) Lateral flow aptamer assay integrated smartphone-based portable device for simultaneous detection of multiple targets using upconversion nanoparticles. Sens Actuators, B 276:48–56. https://doi.org/10.1016/j.snb.2018.08.074
28. Ammanath G, Yeasmin S, Srinivasulu Y, Vats M, Cheema JA, Nabilah F, Srivastava R, Yildiz UH, Alagappan P, Liedberg B (2019) Flow-through colorimetric assay for detection of nucleic acids in plasma. Anal Chim Acta 1066:102–111. https://doi.org/10.1016/j.aca.2019.03.036
29. Liu Q, Li L, Zhao Y, Chen Z (2018) Colorimetric detection of DNA at the nanomolar level based on enzyme-induced gold nanoparticle de-aggregation. Microchim Acta 185:1–6. https://doi.org/10.1007/s00604-018-2833-3
30. Porchetta A, Ippodrino R, Marini B, Caruso A, Caccuri F, Ricci F (2018) Programmable nucleic acid nanoswitches for the rapid, single-step detection of antibodies in bodily fluids. J Am Chem Soc 140:947–953. https://doi.org/10.1021/jacs.7b09347